BMC Cardiovascular Disorders

RESEARCH

Open Access

Identification of hub targets involved in carotid atherosclerosis through bioinformatics and machine learning approaches

Luyao Jia[1], Chunjing Bian[1], Yue Chen[1], Yu Zhao[1], Bin Yang[1], Siyu Sun[1] and Tao Luo[1*]

Abstract

Background Carotid atherosclerosis is a kind of systemic atherosclerosis in the carotid arteries. It remains one of the leading causes of ischemic stroke. However, the efficiency of treatment is insufficient. Thus, it is urgent to deepen the understanding of the underlying mechanisms in carotid atherosclerosis, which may facilitate the development of effective therapeutic interventions. Phenotypic switching of vascular smooth muscle cells (VSMCs) is recognized as a central process in atherosclerosis progression. However, the key regulatory genes involved in this process during carotid atherosclerosis are not fully understood.

Methods Three gene expression datasets, GSE43292, GSE100927, and GSE28829 were downloaded from Gene Expression Omnibus (GEO) database, covering carotid atherosclerosis and control groups. we integrated bioinformatics analysis with three machine learning algorithms to identify the hub genes associated with carotid atherosclerosis. Subsequent validation using clinical specimens and murine atherosclerosis confirmed the expression of the hub genes at both the mRNA and protein levels. Furthermore, in vitro phenotypic switching model using human aortic smooth muscle cells (HASMCs) treated with pro-atherogenic stimuli was established to identify the expression of hub genes and to investigate how knockdown of these hub genes in HASMCs influences VSMCs phenotypic switching.

Results Through the integration of bioinformatics analysis and three machine learning algorithms, we identified PALS2 and CASQ2 as consistently downregulated genes in carotid atherosclerotic plaques compared to normal tissues. Gene interaction network analysis suggested that PALS2 and CASQ2 may cooperatively regulate calcium homeostasis and calcification in VSMCs. This finding was further supported by consistent downregulation of both genes in clinical atherosclerotic samples, murine atherosclerosis, and in HASMCs exposed to pro-atherogenic stimuli. Functionally, knockdown of either gene enhanced VSMCs phenotypic switching, calcium deposition and amplifies CREB1 phosphorylation, collectively demonstrating their protective role in mitigating atherosclerosis.

*Correspondence:
Tao Luo
taoluo35@126.com

Full list of author information is available at the end of the article

Conclusions This study identifies PALS2 and CASQ2 as novel regulators involved in the VSMCs phenotypic switching and calcification in carotid atherosclerosis. Both genes are consistently downregulated in atherosclerotic plaques and function as upstream suppressors of a calcium-CREB1 calcification axis. These findings provide novel insights into the molecular mechanisms of atherosclerosis and highlight PALS2 and CASQ2 as potential therapeutic targets for intervention.

Keywords Atherosclerosis, Vascular smooth muscle cells, Phenotypic switching, Vascular calcification, Machine learning

Introduction

Atherosclerosis is a chronic inflammatory condition characterized by lipid accumulation, vascular dysfunction, and plaque formation [1, 2]. It is the predominant underlying cause of carotid artery disease, which remains one of the leading causes of ischemic stroke [3, 4]. In recent years, the incidence of this disease has significantly increased worldwide and shown a trend toward affecting younger individuals [4, 5]. The management of carotid atherosclerosis primarily encompasses a multifaceted approach, incorporating pharmacological interventions, surgical procedures, and lifestyle modifications. However, many patients still experience disease progression and poor prognosis. Previous research identified vascular smooth muscle cells (VSMCs) as the key cell type in atherosclerotic plaques [6]. During the progression of atherosclerosis, VSMCs experience phenotypic switching, transitioning from a quiescent, low-proliferative contractile phenotype to a highly proliferative, secretory synthetic phenotype, with decreased expression of differentiation markers like α-SMA, SM22α, and SM-MHC [7, 8]. This phenotypic switching has long been considered of fundamental importance to atherosclerosis and plaque stability [7, 9]. However, the mechanisms of phenotypic switching have not yet been fully elucidated. Therefore, identifying the hub genes involved in the phenotypic switching of VSMCs is crucial for improving early diagnosis and developing more effective interventions for carotid atherosclerosis.

The rapid advancements in bioinformatics and machine learning have facilitated the systematic investigation of gene expression profiles in atherosclerotic plaques [10–18]. However, the lack of robust validation and mechanistic exploration hinders the clinical translation of the biomarkers and potential hub genes previously developed. Moreover, the functional interaction between candidate hub genes and the phenotypic switching of VSMCs remains systematically uncharacterized, representing a critical knowledge gap in atherosclerosis progression.

In this study, we integrated bioinformatics analysis with three machine learning algorithms to identify PALS2 and CASQ2 as consistently downregulated genes in carotid atherosclerotic plaques compared to normal tissues. This finding was corroborated by validation across multiple models, including clinical atherosclerotic samples, murine atherosclerotic aortas, and human aortic smooth muscle cells (HASMCs) exposed to diverse pro-atherogenic stimuli. Functionally, knockdown of either gene promoted HASMCs phenotypic switching, increased calcium deposition, and amplified CREB1 phosphorylation, collectively demonstrating their protective role in mitigating atherosclerosis. Mechanistically, both genes converge on the CREB1 signaling axis, positioning them as potential biomarker candidates and therapeutic targets for further investigation.

Methods

Data collection

The transcriptome data of carotid atherosclerosis tissues were acquired from the Gene Expression Omnibus (GEO) database (https://www.ncbi.nlm.nih.gov/geo/). After screening, datasets GSE43292 (12 macroscopically intact tissues / 29 carotid atherosclerosis tissues), GSE100927 (32 normal arterial tissues / 32 carotid atherosclerosis tissues), and GSE28829 (13 early carotid atherosclerosis tissues / 16 advanced carotid atherosclerosis tissues) were selected for analysis. The dataset GSE43292 was designated as the training set, whereas GSE100927 and GSE28829 were utilized as the validation sets. The R package "limma" (version 3.60.0) was employed to mitigate batch effects in the datasets and to perform data normalization.

Data processing and differential expression analysis

Data analysis was conducted using R (version 4.4.0), employing the "GEOquery" package (version 2.72.0) to extract gene expression profiles and associated clinical data. To identify the differential expression genes (DEGs) associated with carotid atherosclerosis, R package "limma" (version 3.60.0) was utilized to obtain the DEGs in carotid atherosclerosis and control samples from the training set. A differential expression threshold was set at $P < 0.01$ and $|\text{Log2 Fold Change (Log2FC)}| > 1$. Significantly up-regulated and down-regulated DEGs in carotid atherosclerosis samples were visualized in the volcano plot, created using the "EnhancedVolcano" package (version 1.22.0) in R.

Gene set enrichment analysis and functional enrichment analysis

Gene set enrichment analysis (GSEA) was performed using the "clusterProfiler" package (version 4.6.0) and the "org.Hs.eg.db" package (version 3.16.0) to identify the differences in pathways between carotid atherosclerosis and controls. Gene ontology (GO) and kyoto encyclopedia of genes and genomes (KEGG) pathway enrichment analyses were performed by DAVID Bioinformatics Resources 6.8 (http://david.abcc.ncifcrf.gov/). The results were visualized with bubble and bar charts created with the "ggplot2" package (version 3.4.1).

Machine learning

Least absolute shrinkage and selection operator (LASSO), support vector machine recursive feature elimination (SVM-RFE) and random forest (RF) were employed using the "glmnet" package (version 4.1-9), the "e1071" package (version 1.7–16) and the "randomForest" package (version 4.7–1.2) to screen key genes from the DEGs, respectively. DEGs were initially screened using the LASSO algorithm. The optimal penalty parameter (λ) was determined through 10-fold cross-validation, employing the minimum mean squared error (MSE) criterion to define the most parsimonious model fit. The number of genes at the point of smallest cross-validation error was designated as the number of disease signature genes. In the case of SVM-RFE, a 5-fold cross-validation strategy was implemented within the recursive feature elimination process to rank gene importance and ascertain the optimal feature subset. The algorithm produced a cross-validation error plot, where the horizontal axis represented the number of candidate genes and the vertical axis ("10× CV Error") indicated the error rate following 10-fold cross-validation. Subsequently, a RF model was constructed with 500 decision trees (ntree = 500). The optimal number of trees was identified by locating the point of minimal cross-validation error. Gene importance scores were calculated based on this optimized model, and genes with importance scores > 1 were selected for further analysis. The intersection of genes identified by all three algorithms was determined and the Venn diagram was plotted using the "VennDiagram" R package (version 1.7.3).

Gene interaction network construction

Utilizing the GeneMANIA tool (http://genemania.org/), we developed hypothetical gene interaction networks for 20 genes, centering on the hub genes PALS2 and CASQ2. The inner circle represents the hub genes, whereas the outer circle comprises the predicted genes.

Receiver Operator Characteristic (ROC) curves and expression of target genes

Wilcoxon tests and univariate logistic regression analyses were performed on carotid plaque tissues and control samples from the GSE43292, GSE100927, and GSE28829 datasets to further validate the expression levels of the identified target genes. Box plots and forest plots were subsequently generated using the "ggplot2" package (version 3.5.2) and the "forestploter" package (version 1.1.3) for visualization respectively. Thereafter, ROC curves for each target gene were constructed utilizing the R package "pROC" (version 1.18.5) to assess the efficacy of the genes in differentiating between carotid atherosclerosis and control samples. Genes that exhibited an area under the curve (AUC) exceeding 0.7 were subsequently identified as potential diagnostic biomarkers for carotid atherosclerosis.

Calibration and Decision Curve Analysis (DCA)

To evaluate the predictive performance and clinical utility of the identified hub genes, calibration curves and DCA were constructed utilizing the R package "rms" (version 8.1-1) and "rmda" (version 1.6), respectively. Calibration curves evaluated the agreement between predicted and observed outcomes, while DCA quantified the net benefit across threshold probabilities.

Sample collection

Ten patients diagnosed with carotid atherosclerosis and underwent carotid endarterectomy (CEA) at the Xuanwu Hospital of Capital Medical University in China were included in the study. The atherosclerotic plaques served as the experimental group, with adjacent macroscopically normal tissues as controls. The research protocol was approved by the Xuanwu Hospital of Capital Medical University. All experiments were conducted by the principles and regulations formulated by the ethics committee. Every participant has signed an informed consent form.

Mouse studies

$Ldlr^{-/-}$ mice (Cat. NO. NM-KO-210198) were purchased from Shanghai Model Organisms Center. Animal care and handling were conducted in accordance with the policies promulgated by the Ethics Committee of the Laboratory Animal Center, Xuanwu Hospital, Capital Medical University, China. To establish an atherosclerosis model, select 8-week-old $Ldlr^{-/-}$ mice and administer a Western diet (D12079B, Research Diets, USA) for a duration of 16 weeks. After that, mice were euthanized for analysis.

Oil red O staining

Whole aortas were extracted from euthanized mice, with all surrounding adipose tissues meticulously removed.

The cleaned aortas were then fixed in 4% PFA at 4 °C overnight. Following fixation, the aortas were longitudinally sectioned and affixed to dissecting dishes with the lumen side facing upwards. The en face aortas were stained with 0.25% Oil Red O (ORO) for 1 h, visualized using a stereomicroscope, and images were captured with a camera.

HASMCs culture and induction of calcification

HASMCs were procured from Procell Technology (CP-H081) and cultured in a complete HASMC medium (CM-H081) within an incubator maintained at 37 °C and under 95% air and 5% CO2 conditions. To induce calcification, the HASMCs were treated with calcification medium, which consisted of high-glucose Dulbecco's Modified Eagle Medium (DMEM) (4.5 g/L) supplemented with 10% FBS, 10 mM β-glycerophosphate (HY-D0886, MedChemExpress), and 5 mM CaCl2 (ST365, Beyotime) for a duration of 7 days. To enhance the generalizability of our conclusions, HASMCs were exposed to Human PDGF-BB Recombinant Protein (PDGF-BB, 100-14B-10UG, Thermo Fisher) at a concentration of 20 ng/mL for 48 h, or Oxidized Low Density Lipoprotein (oxLDL, IO1300, Solarbio) at a concentration of 100 μg/mL for 7 days to induce phenotypic switching. The medium was refreshed every 48 h. Calcium deposition was subsequently visualized using a calcium assay kit (S1063S, Beyotime) and Alizarin Red S (ARS) staining (G1450, Solarbio).

Alizarin red staining

The calcification of HASMCs was assessed using ARS staining in accordance with established protocols. Initially, the cultured HASMCs were washed twice with PBS and subsequently fixed in 4% paraformaldehyde (PFA) for 15 min. Following fixation, the paraformaldehyde was removed, and the cells were washed three times with distilled water. The cells were then exposed in ARS staining solution (0.2%, pH 8.3) for 30 min at room temperature, after which they were washed again with distilled water. Positively stained HASMCs exhibited a reddish coloration, indicating the presence of calcification.

Calcium content detection

Calcium concentrations were quantified utilizing a calcium colorimetric assay kit (S1063S, Beyotime), following the manufacturer's protocol. In brief, an equal number of cells were cultured in 6-well plates and subsequently washed with PBS. A volume of 100 μL of lysis buffer was added to each well, and following cell lysis, the supernatant was collected for further analysis. The detection working solution was then added to both the calcium standards and the samples. The plates were incubated at room temperature in the dark for 10 min. Absorbance at 575 nm was measured using an enzyme reader to generate a standard curve, which was employed to calculate the calcium content in the samples (μg/μL).

Quantitative real-time PCR analysis

Total RNA was isolated from human/mouse aortic tissue and HASMCs utilizing the Trizol Reagent (15596026CN, Thermo Fisher Scientific) in accordance with the manufacturer's protocol. Subsequently, cDNA was synthesized from the total RNA using the Reverse Transcription Kit (BL699A, Biosharp). Quantitative real-time PCR was conducted employing the SYBR Green qPCR Master Mix (HY-K0501A, MedChemExpress), and data acquisition and analysis were performed using the LightCycler 480 II system (Roche). Relative quantification was determined using the $2^{-\Delta\Delta Ct}$ method, with GAPDH serving as the reference gene. Three independent experiments were conducted to calculate the mean values. The sequences of the primers used are provided in Supplemental Table S1.

Protein extraction and western blotting

Proteins from aortic tissue and HASMCs were extracted utilizing RIPA lysis buffer supplemented with protease inhibitor. The protein concentration was determined using BCA standard curve. Equal amounts of protein extracts were subjected to 10% sodium dodecyl sulfate-polyacrylamide gel electrophoresis (SDS-PAGE) and subsequently transferred electrophoretically to polyvinylidene difluoride (PVDF) membranes (Millipore). The membranes were blocked in TBST containing 5% skimmed milk at room temperature for 1 h. Following three washes with TBST, the blocked membranes were incubated with the primary antibody at 4 °C overnight. After three consecutive 10-minute washes with TBST, the membranes were incubated with horseradish peroxidase (HRP)-conjugated goat anti-rabbit or goat anti-mouse secondary antibody for 1 h. The membranes were then washed three additional times with TBST and developed using the ECL+ detection system. The intensity of each strip was measured with ImageJ software. Antibodies are used as follows: PALS2 (abs111889, 1:1000; Absin), CASQ2 (HA721944, 1:1000; HUABIO), α-SMA (ET1607-53, 1:10000; HUABIO), SM22α (abs117418, 1:1000; Absin), OPN (22952-1-AP, 1:2000; Proteintech), RUNX2(20700-1-AP,1:2000; Proteintech), and GAPDH (60004-1-Ig, 1:5000; Proteintech).

Immunofluorescent staining

Aortic tissues were fixed in 4% PFA overnight at 4 °C and subsequently dehydrated using 10%, 20%, and 30% sucrose solutions for 24 h. The specimens were then embedded in an optimal cutting temperature compound (Sakura Finetek, USA) and sectioned at a thickness of 8 μm. HASMCs cultured on coverslips were fixed with 4% PFA for 20 min. Both fixed tissues and cells were

permeabilized with 0.5% Triton X-100 for 15 min at room temperature. Subsequently, 3% BSA solution was applied to block at room temperature for 60 min. The tissues and cells were then incubated with primary antibodies overnight at 4 °C. The primary antibodies utilized were PALS2 (abs111889, 1:500; Absin), CASQ2 (HA721944, 1:500; HUABIO), and α-SMA (ET1607-53, 1:500; HUABIO). After washing thrice with PBS, the tissues and cells were incubated with goat anti-mouse (RGAM002, 1:500; Proteintech) and goat anti-rabbit (RGAR004, 1:500; Proteintech) secondary antibodies for 1 h. Nuclear labeling was performed using DAPI. Images of the immunostained sections were acquired using a confocal microscope (MICA, Leica). The immunohistochemical signal intensity and the positively stained areas of the tissue sections were assessed using ImageJ software.

siRNAs-mediated gene knockdown

HASMCs were transfected with either PALS2 or CASQ2 siRNAs using Lipofectamine RNAiMAX Transfection Reagent (13778150, Thermo Fisher). Efficient knockdown of the target genes was validated by both western blotting and qPCR. The scramble siRNAs were also transfected as negative control. The siRNAs were synthesized by Genepharma (Suzhou, China). The siRNAs sequence targeting PALS2 is 5'-UUUGGAAUCUUCUAGCCUCT T-3'. The siRNAs sequence targeting CASQ2 is 5'-AAUG CGUUCGAAGGCUUGGTT-3'.

Statistical analysis

The datasets were analyzed utilizing RStudio (version 4.5.0). Differential expression analysis was conducted using the student's t-test. Statistical analyses of in vitro experiments were performed with GraphPad Prism 9. Data are presented as mean ± standard deviation (SD). Comparisons between two groups were made using Student's unpaired t-test, while analyses involving multiple groups were conducted using one-way analysis of variance (ANOVA) followed by Tukey's post-hoc test. A P value of less than 0.05 was considered statistically significant.

Results

Identification of DEGs in carotid atherosclerosis and functional enrichment analysis

Three GEO datasets, GSE43292 (12 macroscopically intact tissues / 29 carotid atherosclerosis tissues), GSE100927 (32 normal arterial tissues / 32 carotid atherosclerosis tissues), and GSE28829 (13 early carotid atherosclerosis tissues / 16 advanced carotid atherosclerosis tissues) were analyzed. Differential expression analysis revealed a total of 89 DEGs that exhibited significant alterations in the carotid atherosclerosis samples. Among these, 48 genes were significantly upregulated, while 41 genes were significantly downregulated (Supplementary Table S2). The DEGs are visually represented through volcano plots and heatmaps (Fig. 1A-B).

The functional enrichment analysis was subsequently performed using GSEA, GO and KEGG pathway analysis, respectively. GSEA results revealed that pathways associated with vascular inflammation and lipid metabolism, including the NOD-like receptor signaling pathway, chemokine signaling pathway, and lipid and atherosclerosis pathway, were significantly enriched in the carotid atherosclerosis samples (Fig. 1C-D). Furthermore, the results of GO enrichment analysis indicated that the DEGs were significantly associated with calcium ion homeostasis and its intracellular regulation, including the sequestering and controlled release of calcium ions into the cytosol, particularly from the sarcoplasmic reticulum (Fig. 1E). The KEGG pathway enrichment analysis revealed that the DEGs were significantly enriched in pathways related to signaling molecules and interactions (Fig. 1F).

Collectively, these findings further elucidate that the onset and progression of atherosclerosis are intricately linked to vascular inflammation, lipid metabolism, and immune regulation.

Identification of potential hub genes in carotid

In order to identify the potential hub genes associated with carotid atherosclerosis, three machine learning algorithms were performed. Initially, LASSO regression analysis was utilized for dimensionality reduction, and 5 independent genes (PALS2, FHL5, CASQ2, IBSP, JCHAIN) were identified (Fig. 2A). Next, the SVM-RFE algorithm was utilized to select 15 potential biomarkers from DEGs through 10-fold cross-validation (ITGB2, PALS2, TDO2, GRIA1, MME, ITGAM, PRDM1, GRIA2, NEGR1, CXCL10, FREM1, DPP4, PCDH20, CASQ2, ATP6V0D2) (Fig. 2B). Finally, the RF algorithm was applied to determine the 15 most significant genes with minimal cross-validation error (FHL5, CNN1, TDO2, CASQ2, NEGR1, PALS2, IBSP, FABP4, CNTN4, MMRN1, DPP4, SELE, IL31RA, PLD5, LINC00670) (Fig. 2C). After that, the intersection of the genes screened by three algorithms, PALS2 (MPP6) and CASQ2, was identified as the potential hub genes for further analysis (Fig. 2D).

To further determine the central role of PALS2 and CASQ2 in carotid atherosclerosis, the gene interaction networks were generated using GeneMANIA, and 20 potential genes (CASQ1, RYR1, RYR2, TRDN, RYR3, CLIC3, CADM3, LIN7C, EPB41L2, LIN7B, CEP128, SNX9, CORO2A, PRKCB, RASIP1, OPTN, MRPL3, DES, RBM10, LIN7A) that interact with PALS2 and CASQ2 were identified (Fig. 2E). These genes are predominantly

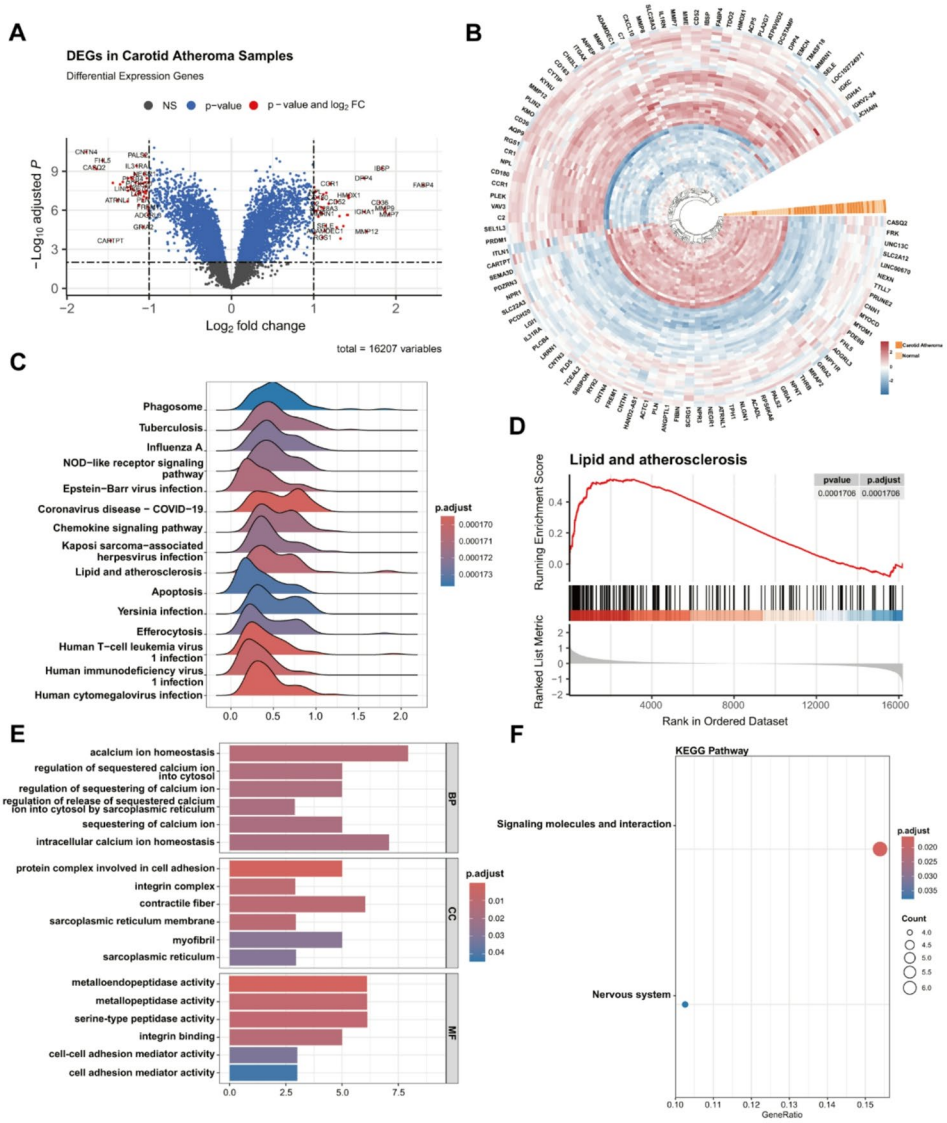

Fig. 1 Identification of candidate genes associated with carotid atherosclerosis. **A** Volcano plot of DEGs in carotid artery atherosclerosis patients. **B** Circular heatmap of 48 upregulated genes and 41 downregulated genes in carotid artery atherosclerosis patients. **C** Ridgeline Plot of gene set enrichment analysis for DEGs. **D** DEGs are significantly enriched in lipid and atherosclerosis pathways. **E** GO enrichment analysis for DEGs. **F** KEGG pathway enrichment analysis for DEGs

associated with functions related to calcium ion transport and chelation.

Expression levels and diagnostic potential of PALS2 and CASQ2

To validate the expression of potential hub genes, Wilcoxon tests and univariate logistic regression analyses were performed on the GSE43292, GSE100927, and GSE28829 datasets. The expression levels of PALS2 and CASQ2 were found to be significantly downregulated in carotid plaque tissues compared to normal arterial tissues. Additionally, the expression of PALS2 and CASQ2 was further decreased in advanced plaques compared to early-stage plaques in the carotid arteries (Figs. 2F and 3A). ROC curves were employed to evaluate the diagnostic accuracy of these two genes across three distinct datasets. Within the training dataset (GSE43292), the AUC values for PALS2 and CASQ2 were 0.903 and 0.895, respectively. In the validation datasets (GSE100927 and GSE28829), PALS2 exhibited AUC values of 0.876 and 0.817, while CASQ2 demonstrated AUC values of 0.871 and 0.788, respectively (Fig. 3B-C). Both genes also showed favorable diagnostic performance in terms of accuracy, sensitivity, and specificity (Supplementary Tables S3 and S4). Furthermore, the calibration curves demonstrated good agreement between predicted and observed outcomes (Supplemental Fig. 1C). DCA revealed positive net benefit across a wide range

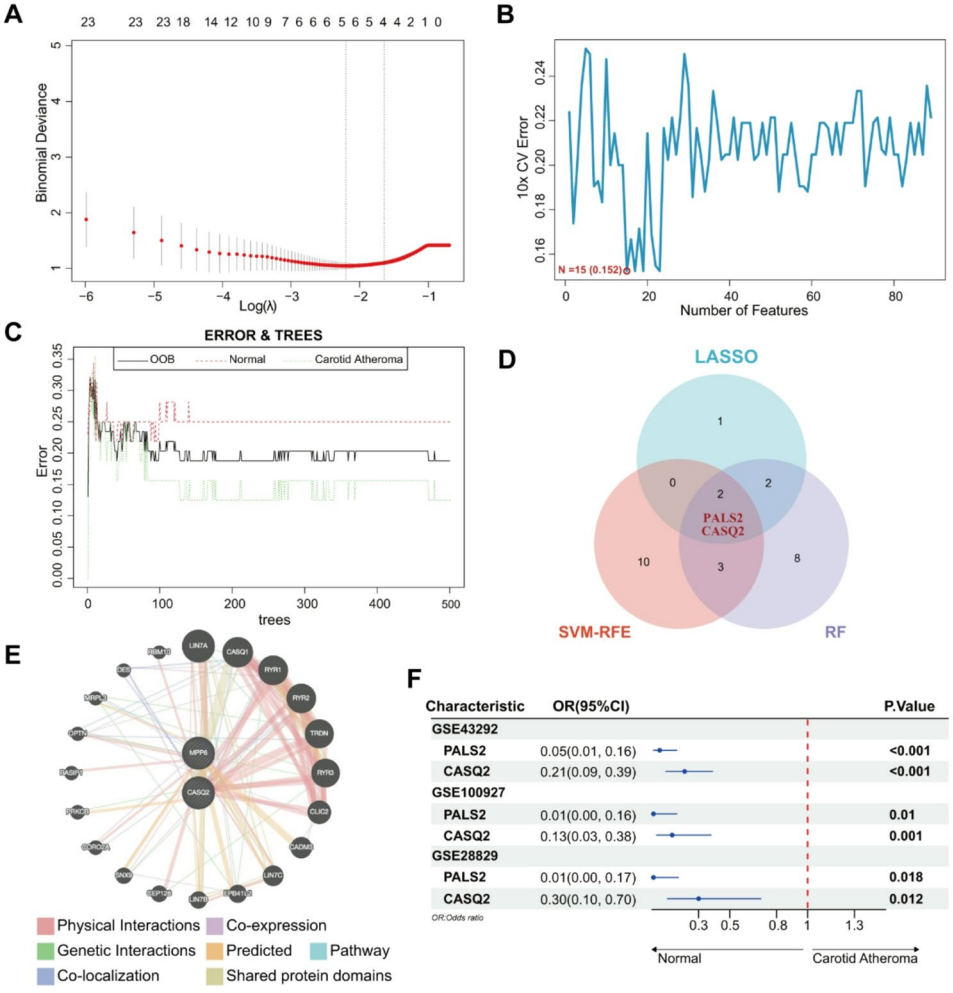

Fig. 2 Construction of target genes based on three machine learning algorithms. **A** LASSO regression analysis. The selection process of the optimum value of the parameter λ in the Lasso regression model by cross-validation method. **B** SVM-RFE algorithm determined 15 target genes with the lowest error rate (0.152). **C** The relationship between the number of Random Forest Trees and the error rate. **D** Venn diagram of the target genes obtained by the three algorithms. **E** Gene-gene interaction network of target genes analyzed using GeneMANIA, showing the top 20 most frequently altered neighboring genes. **F** Forest plot of the odds ratio of target genes associated with carotid artery atherosclerosis

of threshold probabilities (Supplemental Fig. 1D). Thus, our results demonstrated strong diagnostic potential for these two genes, and also suggested the crucial role in preventing carotid atherosclerosis.

Downregulation of PALS2 and CASQ2 in human carotid atherosclerotic plaques and an animal model of atherosclerosis

To validate the bioinformatic predictions, we initially examined the expression levels of PALS2 and CASQ2 in clinical specimens. Human carotid atherosclerotic plaques showed a marked downregulation of both PALS2 and CASQ2 at mRNA and protein levels compared to adjacent normal arterial tissues (Fig. 4A-C). Immunofluorescence staining results indicated that both PALS2 and CASQ2 were highly expressed in normal arterial tissues, mainly in the VSMCs (Fig. 4D-E), while a significant decrease of PALS2 and CASQ2 expression was observed in human carotid plaques relative to the control arterial tissues (Fig. 4D-F). To further substantiate these findings in a controlled experimental setting, we assessed their expression in an established mouse model of atherosclerosis ($Ldlr^{-/-}$ mice fed a western diet for 16 weeks). Consistent with the human data, both PALS2 and CASQ2 were significantly downregulated at the mRNA and protein levels in atherosclerotic aortas compared to those from normal diet-fed control mice (Fig. 4G-M). The consistent results obtained from both human clinical samples and an experimental disease model suggest that the alteration of PALS2 and CASQ2 expression in VSMCs may be involved in the pathological process of atherosclerosis.

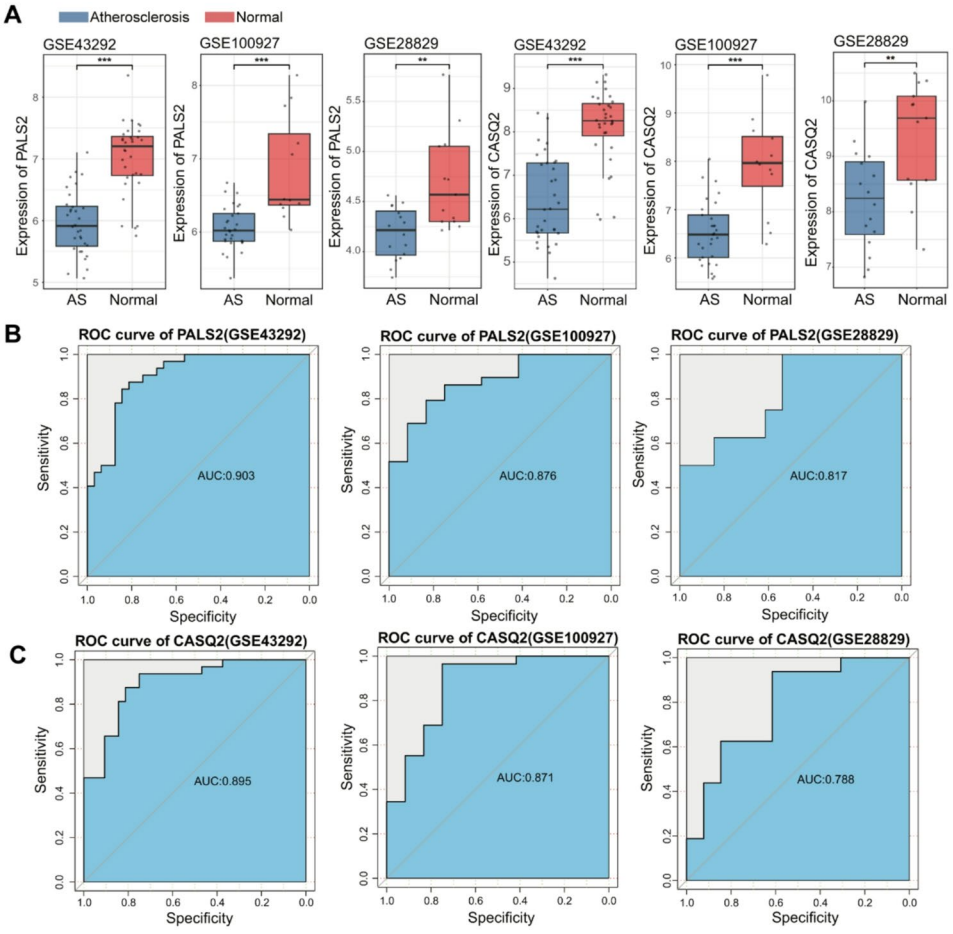

Fig. 3 Validation of target genes as diagnostic biomarkers for carotid atherosclerosis. **A** Expression levels of target genes in three independent atherosclerosis datasets. $^{**}P < 0.01$ and $^{***}P < 0.001$, Student's t-test. **B**, **C** ROC curves for the diagnostic accuracy of target genes in three independent atherosclerosis datasets

Decreased expression of PALS2 and CASQ2 in phenotypic switching of HASMCs

The phenotypic switching of VSMCs represents a pathological process characterized by dedifferentiation, migration, and transdifferentiation into other cell types, constituting a critical event in the progression of atherosclerosis [8]. To better understand the potential role of PALS2 and CASQ2 in atherosclerosis, we monitored their expression during the process of VSMCs phenotypic switching. An in vitro model of HASMCs calcification was applied to induce phenotypic switching of HASMCs. As expected, the expression of contractile VSMCs markers SM22α, α-SMA, and SM-MHC significantly decreased, whereas the expression levels of synthetic phenotype markers, OPN and RUNX2, significantly increased after HASMCs calcification in a time-dependent manner (Fig. 5A-C). Concurrently, the calcium content and calcium deposition in HASMCs progressively increased (Fig. 5D-E). Consistent with the results in human carotid plaques and the mouse model of atherosclerosis (Fig. 4), the expression levels of PALS2 and CASQ2 markedly decreased during VSMCs phenotypic switching (Fig. 5F-G). Notably, the observed downregulation was not confined to the calcification model. Treatment with PDGF-BB or oxLDL also reduced PALS2 and CASQ2 expression in HASMCs (Supplemental Fig. 2A-C). The results of immunofluorescence staining further revealed that PALS2 predominantly localized within the nucleus of HASMCs, whereas CASQ2 was distributed across both the nucleus and cytoplasm (Fig. 5H). Relative fluorescence intensity analysis corroborated the reduction of expression levels of PALS2 and CASQ2 after VSMCs phenotypic switching (Fig. 5H). Thus, the significant decrease of PALS2 and CASQ2 expression in carotid plaques and VSMCs phenotypic switching further suggested that PALS2 and CASQ2 may be hub genes in atherosclerosis.

Deficiency of PALS2 or CASQ2 converges on CREB1 hyperactivation to exacerbate HASMCs calcification

To clarify the causal relationship between the potential hub genes, PALS2 and CASQ2, and atherosclerosis, we

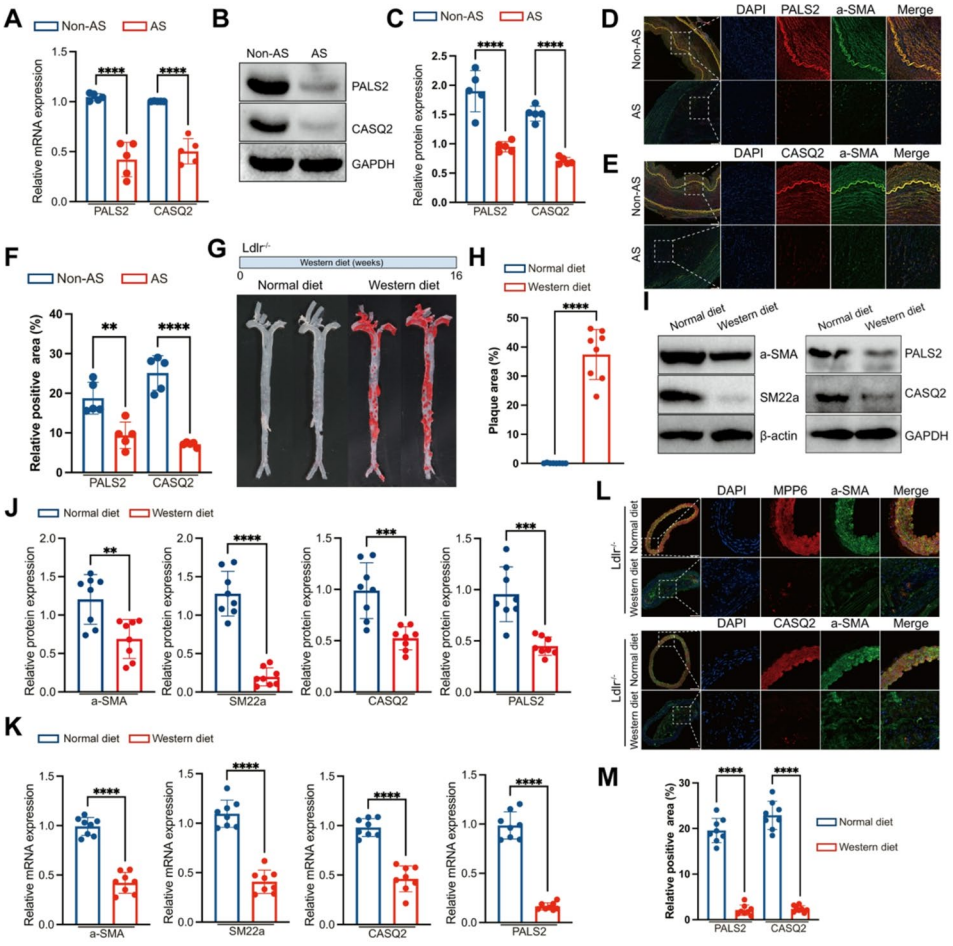

Fig. 4 PALS2 and CASQ2 are downregulated in human carotid atherosclerotic plaques and an animal atherosclerosis model. **A** The mRNA expression of PALS2 and CASQ2 in human carotid atherosclerotic plaques and control samples was determined by qRT-PCR. Data are presented as mean ± SD, $^{****}P < 0.0001$, Student's t-test. $n = 5$. **B**, **C** Western blotting was conducted to confirm the decrease of PALS2 and CASQ2 protein levels in human carotid atherosclerotic plaques. Data are presented as mean ± SD, $^{****}P < 0.0001$, Student's t-test. $n = 5$. **D**, **E** PALS2 and CASQ2 expression level was further examined by immunofluorescence staining. Bar: 500 μm. **F** Quantification of the relative positive area in human carotid atherosclerotic plaques and control samples **(D**, **E)**. Data are presented as mean ± SD, $^{**}P < 0.01$ and $^{****}P < 0.0001$, Student's t-test. $n = 5$. **G** En face Oil Red O staining was performed on aortas from Ldlr$^{-/-}$ mice fed either a western diet (WD) or a normal diet (ND) for 16 weeks. **H** Quantification of the relative positive area in **(G)**. Data are presented as mean ± SD, $^{****}P < 0.0001$, Student's t-test. $n = 8$. **I**, **J** The protein expression of α-SMA, SM22α, PALS2 and CASQ2 in aortas of WD- versus ND-fed Ldlr$^{-/-}$ mice was determined by western blot and quantitated by densitometric analysis. Data are presented as mean ± SD, $^{**}P < 0.01$, $^{***}P < 0.001$, and $^{****}P < 0.0001$, Student's t-test. $n = 8$. **K** The mRNA expression of SM-MHC, α-SMA, SM22α, PALS2 and CASQ2 in aortas of WD- versus ND-fed Ldlr$^{-/-}$ mice was determined by qRT-PCR. Data are presented as mean ± SD, $^{****}P < 0.0001$, Student's t-test. $n = 8$. **L**, **M** Quantification of the relative positive area in aortas of WD- versus ND-fed Ldlr$^{-/-}$ mice **(M)**. Data are presented as mean ± SD, $^{****}P < 0.0001$, Student's t-test. $n = 8$

knock down these two genes in HASMCs, respectively (Supplemental Fig. 2D). Knockdown of PALS2 itself, but not CASQ2, increased the protein levels of OPN and RUNX2 in HASMCs (Fig. 6A-B). Together with the induction of VSMCs calcification, either PALS2 or CASQ2 siRNAs could further increase the expression of OPN and RUNX2 at both mRNA and protein levels in HASMCs compared to the scramble siRNAs. As expected, more reduction in the expression levels of the contractile markers, SM22α and α-SMA, was observed in calcified HASMCs treated with PASL2 or CASQ2 siRNAs compared to scramble siRNAs (Fig. 6A-E). Consistently, PALS2 and CASQ2 siRNAs could further aggravate the calcium content and calcium deposition in HASMCs treated with calcium medium (Fig. 6F-G). Thus, our results indicated that both PALS2 and CASQ2 may play key roles in preventing HASMCs from phenotypic switching in atherosclerosis, probably through different signaling pathways.

To further elucidate the functional roles of PALS2 and CASQ2 in vascular calcification and explore the underlying calcium ion homeostasis and its intracellular regulation mechanisms, we monitored the expression of p-CREB1/CREB1 during the process of VSMCs phenotypic switching. Our in vitro calcification model, utilizing HASMCs induced by a calcification medium, revealed

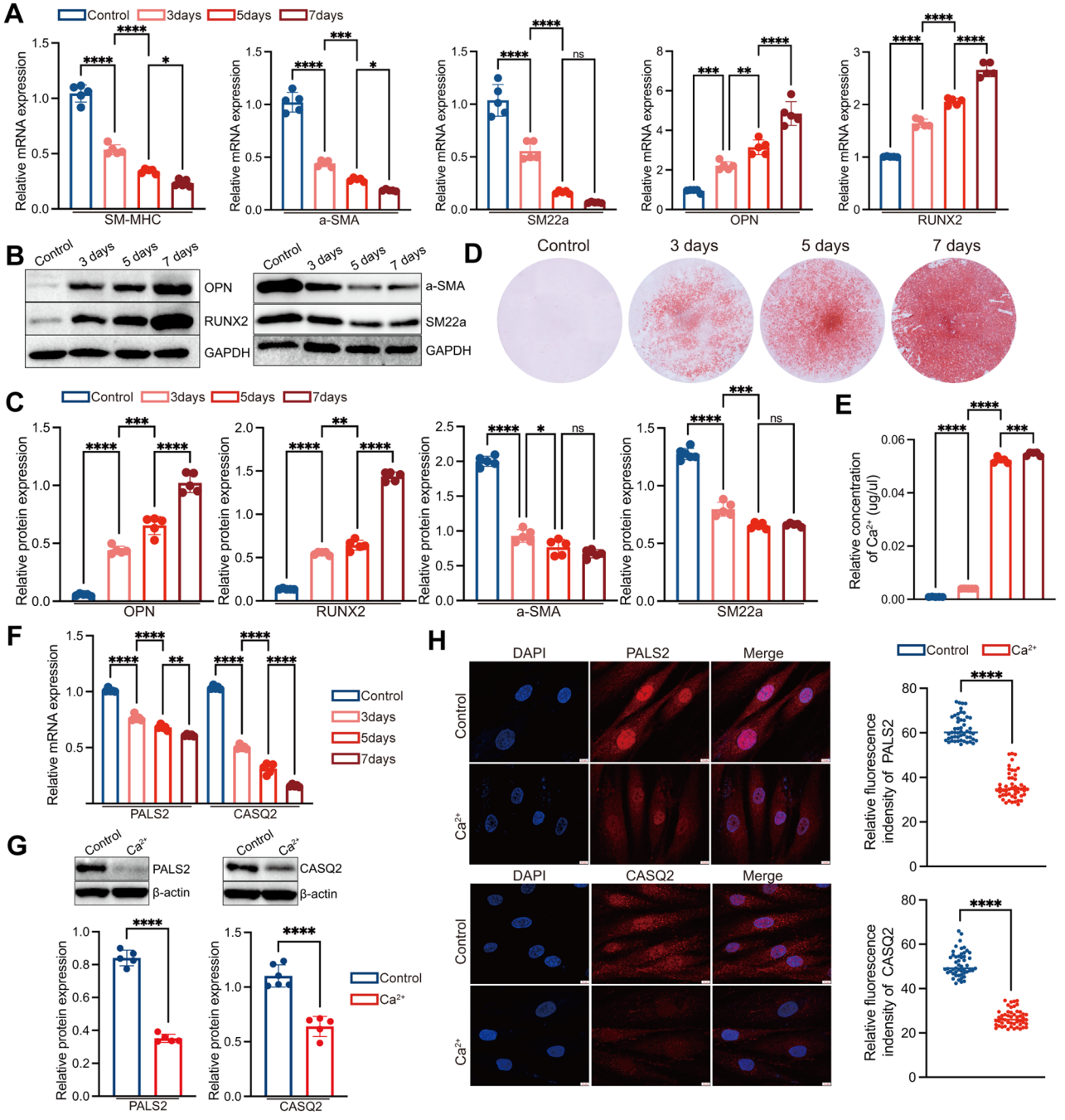

Fig. 5 PALS2 and CASQ2 expression is significantly reduced in calcified HASMCs. HASMCs were treated with high-phosphate and $CaCl_2$ medium for 0, 3, 5, or 7 days **(A-H)**. **A** The key markers of vascular calcification and contractile VSMCs were examined using qRT-PCR. Data are presented as mean ± SD, $^{*}P < 0.05$, $^{**}P < 0.01$, $^{***}P < 0.001$, and $^{****}P < 0.0001$. ns: not significant. one-way ANOVA. $n = 5$. **B**, **C** The expression of OPN, RUNX2, α-SMA, and SM22α was determined by western blot and quantitated by densitometric analysis. Data are presented as mean ± SD, $^{*}P < 0.05$, $^{**}P < 0.01$, $^{***}P < 0.001$, and $^{****}P < 0.0001$. ns: not significant. one-way ANOVA. $n = 5$. **D**, **E** Calcium content was quantified, and mineralization was assessed by Alizarin Red S staining. Data are presented as mean ± SD, $^{***}P < 0.001$ and $^{****}P < 0.0001$. one-way ANOVA. $n = 5$. **F** The mRNA expression of PALS2 and CASQ2 was determined by qRT-PCR. Data are presented as mean ± SD, $^{**}P < 0.01$ and $^{****}P < 0.0001$. one-way ANOVA. $n = 5$. **G** The expression of PALS2 and CASQ2 was determined by western blot. Data are presented as mean ± SD, $^{**}P < 0.01$ and $^{****}P < 0.0001$. one-way ANOVA. $n = 5$. **H** PALS2 and CASQ2 expression level was further examined by immunofluorescence staining. Bar: 10 μm. Fifty cells in each group were analyzed by ImageJ. Data are presented as mean ± SD, $^{****}P < 0.0001$. Student's t-test. $n = 5$

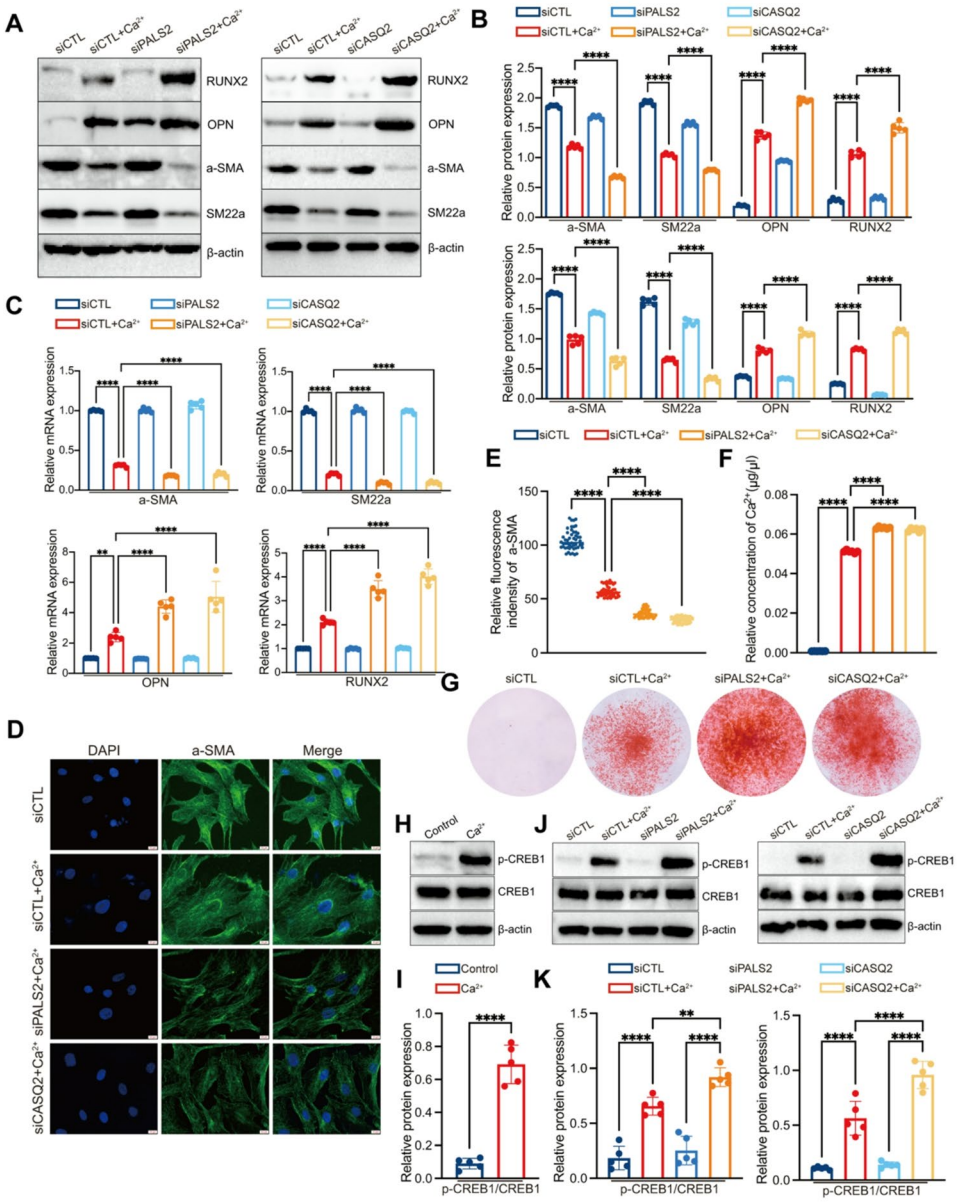

Fig. 6 Down-regulation of PALS2 or CASQ2 promotes calcification and phenotypic switching in HASMCs. HASMCs transfected with either control siRNA (siCTL), PALS2 and CASQ2 specific siRNA (siPALS2 or siCASQ2) were treated with high-phosphate and $CaCl_2$ medium for 5 days **(A-G)**. **A**, **B** The expression of α-SMA, SM22α, OPN and RUNX2 was determined by western blot. Data are presented as mean ± SD, ****$P < 0.0001$. one-way ANOVA. $n = 5$. **C** The key markers of vascular calcification and contractile VSMCs were examined using qRT-PCR. Data are presented as mean ± SD, **$P < 0.01$ and ****$P < 0.0001$. one-way ANOVA. $n = 5$. **D**, **E** The expression of α-SMA was further examined by immunofluorescence staining. Bar: 10 μm. Fifty cells in each group were analyzed by ImageJ. Data are presented as mean ± SD, ****$P < 0.0001$. Student's t-test. $n = 5$. **F** The key markers of vascular calcification and contractile VSMCs were examined using qRT-PCR. Data are presented as mean ± SD, **$P < 0.01$ and ****$P < 0.0001$. one-way ANOVA. $n = 5$. **G** The mineralization was assessed by Alizarin Red S staining. **H**, **I** Human VSMCs were treated with high-phosphate and $CaCl_2$ medium for 5 days. The expression of p-CREB1/CREB1 was determined by western blot. Data are presented as mean ± SD, ****$P < 0.0001$. Student's t-test. $n = 5$. **J**, **K** HASMCs transfected with either control siRNA (siCTL), PALS2 and CASQ2 specific siRNA (siPALS2 or siCASQ2) were treated with high-phosphate and $CaCl_2$ medium for 5 days. The expression of p-CREB1/CREB1 was determined by western blot. Data are presented as mean ± SD, **$P < 0.01$ and ****$P < 0.0001$. one-way ANOVA. $n = 5$

a significant increase in the levels of p-CREB1, indicating activation of the CREB signaling pathway (Fig. 6H-I). Notably, knockdown of PALS2 or CASQ2 exacerbated calcification and further elevated the expression of p-CREB1/CREB1 (Fig. 6J-K).

Discussion

This study provides novel insights into the molecular mechanisms underlying atherosclerosis by integrating bioinformatics analysis with machine learning algorithms and experimental validation across multiple models. Our

findings highlight the critical role of VSMCs phenotypic switching in disease progression and identify PALS2 and CASQ2 as potential regulators of this process through convergent activation of the CREB1 signaling axis, positioning them as promising candidates for further investigation as diagnostic biomarkers and therapeutic targets.

The identification of 89 DEGs in carotid atherosclerotic plaques compared to control artery tissues reveals significant alterations in biological pathways associated with disease pathogenesis. Notably, GSEA analysis demonstrated strong associations with vascular inflammation and lipid metabolism, consistent with previous studies about the mechanisms of atherosclerosis development [2, 19, 20]. The specific enrichment of calcium ion homeostasis and its intracellular regulation pathways further suggests that impaired intracellular calcium buffering within vascular smooth muscle cells may be a key mechanism contributing to their phenotypic switching and to the progression of plaque calcification, thereby offering novel mechanistic insights into disease pathogenesis. The gene interaction networks demonstrated that the genes associated with PALS2 and CASQ2 are primarily involved in pathways related to calcium ion transport and chelation. Calcium homeostasis is associated with atherosclerosis [21], and fluctuations of calcium ions within VSMCs can affect cell proliferation, migration, and phenotypic transformation [22, 23]. This suggests that PALS2 and CASQ2 may collaboratively regulate calcium homeostasis in vascular smooth muscle cells and participate in the cellular calcification process. Notably, calcification is a hallmark of advanced atherosclerotic plaques and is linked to plaque vulnerability [24, 25]. These findings support the growing recognition that calcium dysregulation may play a pivotal role in vascular pathology.

In recent years, machine learning algorithms have demonstrated superior efficacy in atherosclerosis diagnosis and biomarker discovery, attributed to their enhanced predictive performance, reduced error rates, and improved reliability when compared to traditional methods [11, 13, 26]. Therefore, we applied three machine-learning strategies, LASSO, SVM-RFE coupled with RF, to screen and determine the hub genes of atherosclerosis. By intersecting the genes identified by these three algorithmic approaches, we effectively reduced the number of candidate genes, thereby enhancing the specificity and sensitivity of the identified genetic signatures. Ultimately, our study identified PALS2 and CASQ2 as hub genes for carotid atherosclerosis. We consistently observed the downregulation of both genes in human carotid plaques across multiple independent datasets (GSE43292, GSE100927, GSE28829), with progressive suppression in advanced versus early-stage plaques. Furthermore, the ROC analysis on diagnostic performance demonstrated that PALS2 and CASQ2 could distinguish individuals from atherosclerosis and those without. The calibration curves demonstrated agreement between predicted probabilities and observed outcomes, indicating good model fit. DCA revealed positive net benefit across a wide range of threshold probabilities, supporting the potential clinical usefulness of these genes as diagnostic markers. Importantly, our validation in human carotid plaques and the mouse model of atherosclerosis demonstrated significant downregulation of both PALS2 and CASQ2 at mRNA and protein levels, further indicating their potential protective roles against atherosclerosis pathogenesis. The in vitro experiments provided evidence establishing a causal relationship between PALS2 and CASQ2 and the phenotypic switching of VSMCs. Downregulation of these genes during calcification-induced VSMCs transformation, accompanied by decreased contractile markers and increased osteogenic markers, suggests their crucial role in preserving VSMCs contractility. Notably, treatment with PDGF-BB or oxLDL also reduced PALS2 and CASQ2 expression in HASMCs. The observation demonstrates that downregulation of PALS2 and CASQ2 is a common event in VSMCs phenotypic switching induced by diverse pathological stimuli associated with atherosclerosis. The distinct subcellular localization patterns suggest PALS2 and CASQ2 have different but complementary mechanisms. PALS2 and CASQ2 may play important roles in preventing pathological calcification by modulating intracellular calcium homeostasis, aligning with emerging evidence that suggests calcium dysregulation is a driving factor in the phenotypic switching of VSMCs [27–29].

Previous studies have reported that PALS2 and CASQ2 were involved in the progression of several diseases. CASQ2 (Calsequestrin 2) is a critical component of the RyR2 macromolecular complex, precisely regulating calcium-induced calcium release and preventing diastolic leakage, where loss-of-function mutations are known to cause catecholaminergic polymorphic ventricular tachycardia type 2 (CPVT2) [30–32]. Dong et al. identified CASQ2 as a potential atherosclerosis biomarker through bioinformatics analysis, but it has not been clinically validated [33]. PALS2 (also known as MAGUK P55 Subfamily Member 6, and membrane palmitoylated protein 6, MPP6) is involved in regulating various cell signaling, behavior, and intercellular junctions [34] and is identified as a gene signature of oncogene-induced replication stress [35]. However, no studies have indicated the causal relationship between these two genes and the phenotypic switching of VSMCs as well as atherosclerosis yet. Our findings indicate that CASQ2 serves a distinct, context-dependent function in VSMCs as an intracellular calcium buffer maintaining cytosolic calcium homeostasis. The observed downregulation of CASQ2 in atherosclerotic plaques and calcified VSMCs, along with the

exacerbation of calcification and CREB1 hyperactivation following CASQ2 knockdown, suggests that the loss of CASQ2 impairs calcium buffering capacity. This disruption promotes a pro-calcific, osteogenic gene program, which represents a pathological process of structural remodeling rather than electrical dysfunction. Similarly, our data demonstrate that the knockdown of PALS2 exacerbates calcium deposition and amplifies CREB1 phosphorylation, mirroring the effects of CASQ2 deficiency. We propose that PALS2, functioning as a scaffold protein at cell junctions, may facilitate the maintenance of local signaling complexes that regulate calcium influx or interactions between the sarcoplasmic reticulum and the plasma membrane. The disruption of PALS2 leads to dysregulation of cytosolic calcium levels, which activates calcium/calmodulin-dependent kinases and subsequently results in increased phosphorylation of CREB1, thereby promoting osteogenic gene expression [36–38]. Collectively, PALS2 and CASQ2 converge on a calcium-CREB1 regulatory axis, and their combined downregulation in atherosclerosis potentiates this pathway, accelerating disease progression.

Several limitations should be acknowledged. First, this study is a retrospective analysis based on the GEO dataset. While PALS2 and CASQ2 are consistently downregulated across human plaques, murine atherosclerosis, and HASMCs exposed to pro-atherogenic stimuli, their promise as biomarkers of phenotypic switching or therapeutic response requires large-scale clinical validation. Future studies should also assess whether their plasma or monocyte levels correlate with plaque burden, enabling non-invasive monitoring. Second, the therapeutic potential of strategies aimed at restoring PALS2/CASQ2 expression or modulating downstream CREB1 signaling needs to be evaluated in animal models of atherosclerosis.

Conclusions

This study identifies PALS2 and CASQ2 as novel regulators of VSMCs phenotypic switching and calcification in atherosclerosis by integrating bioinformatics, machine learning, and multi-model experimental validation. Both genes are consistently downregulated in atherosclerotic plaques and function as upstream suppressors of a calcium-CREB1 calcification axis. These findings provide new mechanistic insights into atherosclerosis pathogenesis and establish PALS2 and CASQ2 as potential diagnostic and therapeutic candidates for future investigation.

Abbreviations

VSMCs	Vascular smooth muscle cells
HASMCs	Human aortic smooth muscle cells
SR	Sarcoplasmic reticulum
DEGs	Differential expression genes
GSEA	Gene set enrichment analysis
GO	Gene ontology
KEGG	Kyoto encyclopedia of genes and genomes
LASSO	Least absolute shrinkage and selection operator
SVM-RFE	Support vector machine recursive feature elimination
RF	Random forest
ROC	Receiver operator characteristic
AUC	Area under the curve
CEA	Carotid endarterectomy
DMEM	Dulbecco's Modified Eagle Medium
ARS	Alizarin red s
PFA	Paraformaldehyde
SDS-PAGE	Sodium dodecyl sulfate-polyacrylamide gel electrophoresis
PVDF	Polyvinylidene difluoride

Supplementary Information

The online version contains supplementary material available at https://doi.org/10.1186/s12872-026-05748-2.

Supplementary Material 1.

Supplementary Material 2.

Supplementary Material 3.

Acknowledgements

The authors are grateful to the patients who generously donated artery tissues. Additionally, their appreciation goes out to the GEO database for generously offering their platform and to the contributors for their dedicated efforts in uploading their datasets.

Clinical trial number

Not applicable.

Authors' contributions

Luyao Jia designed the study and wrote the manuscript. Chunjing Bian conceived the study, supervised the experimental work, and revised the manuscript. Yue Chen, Bin Yang, Yu Zhao, and Siyu Sun performed the statistical analyses. Tao Luo conceived and designed the study, supervised the research, and revised the manuscript. All authors approved the final version of the manuscript.

Funding

This work was supported by the National Natural Science Foundation of China (Grant number: 8227021918).

Data availability

The datasets used and analyzed during the current study are available from the corresponding author on reasonable request. Accession numbers of the datasets used in current study are GSE43292, GSE100927 and GSE28829 in Gene Expression Omnibus database (https://www.ncbi.nlm.nih.gov/geo/).

Declarations

Ethics approval and consent to participate

All animal experimental protocols were approved by the Animal Ethics Committee of the Laboratory Animal Center, Xuanwu Hospital, Capital Medical University, China (XW-20210420-1). This study was approved by the Institutional Review Board of the Xuanwu Hospital, Capital Medical University (the approval number [2024]163-001) and complied with the Declaration of Helsinki. All patients provided the written informed consent according to the institutional guidelines.

Consent for publication

Not applicable.

Competing interests

The authors declare no competing interests.

Author details

[1]Department of General Surgery, Xuanwu Hospital, Capital Medical University, Beijing 100053, China

Received: 2 December 2025 / Accepted: 13 March 2026
Published online: 18 March 2026

References

1. Libby P. Inflammation in atherosclerosis [J]. Nature. 2002;420(6917):868–74. https://doi.org/10.1038/nature01323.
2. Libby P. Nature. The changing landscape of atherosclerosis [J]. 2021;592(7855):524–. https://doi.org/10.1038/s41586-021-03392-8.
3. Falk E. Pathogenesis of atherosclerosis [J]. J Am Coll Cardiol. 2006;47(8 Suppl):C7–12. https://doi.org/10.1016/j.jacc.2005.09.068.
4. Fu J, Deng Y, Ma Y, Man S, Yang X, Yu C, et al. National and Provincial-Level Prevalence and Risk Factors of Carotid Atherosclerosis in Chinese Adults [J]. JAMA Netw Open. 2024;7(1):e2351225. https://doi.org/10.1001/jamanetworkopen202351225.
5. Song P, Fang Z, Wang H, Cai Y, Rahimi K, Zhu Y, et al. Global and regional prevalence, burden, and risk factors for carotid atherosclerosis: a systematic review, meta-analysis, and modelling study [J]. Lancet Glob Health. 2020;8(5):e721–9. https://doi.org/10.1016/s2214-109x(20)30117-0.
6. Bennett MR, Sinha S, Owens GK. Vascular Smooth Muscle Cells in Atherosclerosis [J]. Circ Res. 2016;118(4):692–702. https://doi.org/10.1161/circresaha.115.306361.
7. Liu R, Leslie KL, Martin KA. Epigenetic regulation of smooth muscle cell plasticity [J]. Biochim Biophys Acta. 2015;1849(4):448–53. https://doi.org/10.1016/j.bbagrm.2014.06.004.
8. Frismantiene A, Philippova M, Erne P, Resink TJ. Smooth muscle cell-driven vascular diseases and molecular mechanisms of VSMC plasticity [J]. Cell Signal. 2018;52:48–64. https://doi.org/10.1016/j.cellsig.2018.08.019.
9. Wirka RC, Wagh D, Paik DT, Pjanic M, Nguyen T, Miller CL, et al. Atheroprotective roles of smooth muscle cell phenotypic modulation and the TCF21 disease gene as revealed by single-cell analysis [J]. Nat Med. 2019;25(8):1280–9. https://doi.org/10.1038/s41591-019-0512-5.
10. Xie W, Chen S, Luo H, Kong C, Wang D. Critical gene signature and immunological characterization in peripheral vascular atherosclerosis: novel insights from mendelian randomization and transcriptomics [J]. Front Genet. 2024;15:1361445. https://doi.org/10.3389/fgene.2024.1361445.
11. Qin X, Ding R, Lu H, Zhang W, Wei S, Ji B, et al. Identification of pivotal genes and regulatory networks associated with atherosclerotic carotid artery stenosis based on comprehensive bioinformatics analysis and machine learning [J]. Front Pharmacol. 2024;15:1364160. https://doi.org/10.3389/fphar.2024.1364160.
12. Mo L, Ma C, Wang Z, Li J, He W, Niu W. Integrated Bioinformatic Analysis of the Shared Molecular Mechanisms Between Osteoporosis and Atherosclerosis [J]. Front Endocrinol (Lausanne). 2022;13:950030. https://doi.org/10.3389/fendo.2022.950030.
13. Ye Z, Wang XK, Lv YH, Wang X, Cui YC. The Integrated Analysis Identifies Three Critical Genes as Novel Diagnostic Biomarkers Involved in Immune Infiltration in Atherosclerosis [J]. Front Immunol. 2022;13:905921. https://doi.org/10.3389/fimmu.2022.905921.
14. Chen C, Wu Y, Lu HL, Liu K, Qin X. Identification of potential biomarkers of vascular calcification using bioinformatics analysis and validation in vivo [J]. PeerJ. 2022;10:e13138. https://doi.org/10.7717/peerj13138.
15. Zhang W, Wu Y, Yuan Y, Wang L, Yu B, Li X, et al. Identification of key biomarkers for predicting atherosclerosis progression in polycystic ovary syndrome via bioinformatics analysis and machine learning [J]. Comput Biol Med. 2024;183:109239. https://doi.org/10.1016/j.compbiomed.2024.109239.
16. Chen H, Wu B, Guan K, Chen L, Chai K, Ying M, et al. Identification of lipid metabolism related immune markers in atherosclerosis through machine learning and experimental analysis [J]. Front Immunol. 2025;16:1549150. https://doi.org/10.3389/fimmu.2025.1549150.
17. Ke Y, Yue J, He J, Liu G. Integrating machine learning algorithms and single-cell analysis to identify gut microbiota-related macrophage biomarkers in atherosclerotic plaques [J]. Front Cell Infect Microbiol. 2024;14:1395716. https://doi.org/10.3389/fcimb.2024.1395716.
18. Xie Q, Zhang X, Liu F, Luo J, Liu C, Zhang Z, et al. Identification and verification of immune-related genes for diagnosing the progression of atherosclerosis and metabolic syndrome [J]. BMC Cardiovasc Disord. 2024;24(1):405. https://doi.org/10.1186/s12872-024-04026-3.
19. Zhu Y, Xian X, Wang Z, Bi Y, Chen Q, Han X, et al. Research Progress on the Relationship between Atherosclerosis and Inflammation [J]. Biomolecules. 2018;8(3). https://doi.org/10.3390/biom8030080.
20. Kobiyama K, Ley K. Atherosclerosis [J]. Circ Res. 2018;123(10):1118–20. https://doi.org/10.1161/circresaha.118.313816.
21. Zhang Z, Yang F, Wang W, Cao Q, Zhang L, Zhang Y, et al. Cholesterol induced-mitochondrial calcium dysregulation facilitates atherosclerosis by promoting lipid accumulation in vascular smooth muscle cells [J]. Mol Biomed. 2025;6(1):129. https://doi.org/10.1186/s43556-025-00384-2.
22. Scherberich A, Campos-Toimil M, Rondé P, Takeda K, Beretz A. Migration of human vascular smooth muscle cells involves serum-dependent repeated cytosolic calcium transients [J]. J Cell Sci. 2000;113(Pt 4):653–62. https://doi.org/10.1242/jcs.113.4.653.
23. Liu J, Xu S, Gao B, Yuan M, Zhong L, Guo R. Protective effect of SERCA2a-SUMOylation by SUMO-1 on diabetes-induced atherosclerosis and aortic vascular injury [J]. Mol Cell Biochem. 2025;480(1):279–93. https://doi.org/10.1007/s11010-024-04953-x.
24. Durham AL, Speer MY, Scatena M, Giachelli CM, Shanahan CM. Role of smooth muscle cells in vascular calcification: implications in atherosclerosis and arterial stiffness [J]. Cardiovasc Res. 2018;114(4):590–600. https://doi.org/10.1093/cvr/cvy010.
25. Li M, Wang ZW, Fang LJ, Cheng SQ, Wang X, Liu NF. Programmed cell death in atherosclerosis and vascular calcification [J]. Cell Death Dis. 2022;13(5):467. https://doi.org/10.1038/s41419-022-04923-5.
26. Liu C, Zhou Y, Zhou Y, Tang X, Tang L, Wang J. Identification of crucial genes for predicting the risk of atherosclerosis with system lupus erythematosus based on comprehensive bioinformatics analysis and machine learning [J]. Comput Biol Med. 2023;152:106388. https://doi.org/10.1016/j.compbiomed.2022.106388.
27. Dai C, Khalil RA. Calcium Signaling Dynamics in Vascular Cells and Their Dysregulation in Vascular Disease [J]. Biomolecules. 2025;15(6). https://doi.org/10.3390/biom15060892.
28. Beckman JA, Ganz J, Creager MA, Ganz P, Kinlay S. Relationship of clinical presentation and calcification of culprit coronary artery stenoses [J]. Arterioscler Thromb Vasc Biol. 2001;21(10):1618–22. https://doi.org/10.1161/hq0901095554.
29. Ehara S, Kobayashi Y, Yoshiyama M, Shimada K, Shimada Y, Fukuda D, et al. Spotty calcification typifies the culprit plaque in patients with acute myocardial infarction: an intravascular ultrasound study [J]. Circulation. 2004;110(22):3424–9. https://doi.org/10.1161/01.Cir.0000148131.41425.E9.
30. Terentyev D, Kubalova Z, Valle G, Nori A, Vedamoorthyrao S, Terentyeva R, et al. Modulation of SR Ca release by luminal Ca and calsequestrin in cardiac myocytes: effects of CASQ2 mutations linked to sudden cardiac death [J]. Biophys J. 2008;95(4):2037–48. https://doi.org/10.1529/biophysj.107.128249.
31. Ng K, Titus EW, Lieve KV, Roston TM, Mazzanti A, Deiter FH, et al. An International Multicenter Evaluation of Inheritance Patterns, Arrhythmic Risks, and Underlying Mechanisms of CASQ2-Catecholaminergic Polymorphic Ventricular Tachycardia [J]. Circulation. 2020;142(10):932–47. https://doi.org/10.1161/circulationaha.120.045723.
32. Liu N, Priori SG. Disruption of calcium homeostasis and arrhythmogenesis induced by mutations in the cardiac ryanodine receptor and calsequestrin [J]. Cardiovasc Res. 2008;77(2):293–301. https://doi.org/10.1093/cvr/cvm004.
33. Dong R, Li J, Jiang G, Han N, Zhang Y, Shi X. Novel immune cell infiltration-related biomarkers in atherosclerosis diagnosis [J]. PeerJ. 2023;11:e15341. https://doi.org/10.7717/peerj.15341.
34. Ivanova S, Gregorc U, Vidergar N, Javier R, Bredt DS, Vandenabeele P, et al. MAGUKs, scaffolding proteins at cell junctions, are substrates of different proteases during apoptosis [J]. Cell Death Dis. 2011;2(1):e116. https://doi.org/10.1038/cddis201092.
35. Guerrero Llobet S, Bhattacharya A, Everts M, Kok K, van der Vegt B, Fehrmann RSN. An mRNA expression-based signature for oncogene-induced replication-stress [J]. Oncogene. 2022;41(8):1216–24. https://doi.org/10.1038/s41388-021-02162-0.
36. Siddappa R, Martens A, Doorn J, Leusink A, Olivo C, Licht R, et al. cAMP/PKA pathway activation in human mesenchymal stem cells in vitro results in robust bone formation in vivo [J]. Proc Natl Acad Sci U S A. 2008;105(20):7281–6. https://doi.org/10.1073/pnas0711190105.
37. Yu W, Chen FC, Xu WN, Ding SL, Chen PB, Yang L, et al. Inhibition of Y1 Receptor Promotes Osteogenesis in Bone Marrow Stromal Cells via cAMP/PKA/CREB Pathway [J]. Front Endocrinol (Lausanne). 2020;11:583105. https://doi.org/10.3389/fendo.2020.583105.

38. Zhou Y, Zhao D, Ma Q, Lee S, Roh K, Cai Y, et al. Targeting adenosine 2A receptor signaling suppresses vascular calcification by restraining smooth muscle osteogenic differentiation [J]. Pharmacol Res. 2025;221:108012. https://doi.org/10.1016/j.phrs.2025.108012.